IET Radar, Sonar & Navigation

Research Article

IET Journals
The Institution of Engineering and Technology

Multi-frequency analysis of Gaussian process modelling for aperiodic RCS responses of a parameterised aircraft model

ISSN 1751-8784
Received on 18th October 2019
Revised 10th March 2020
Accepted on 11th March 2020
E-First on 22nd April 2020
doi: 10.1049/iet-rsn.2019.0421
www.ietdl.org

Ahmad Bilal[1] ✉, *Syed Muhammad Hamza*[1], *Ziauddin Taj*[2], *Shuaib Salamat*[2]

[1]*Department of Avionics Engineering, Air University PAC Campus, Kamra, Pakistan*
[2]*Department of Aerospace Engineering, Air University PAC Campus, Kamra, Pakistan*
✉ *E-mail: ahmadbilal@aerospace.pk*

Abstract: Radar cross-section (RCS) of an object is a complex function of various geometric variables, frequency and angles of incidence. In this work, an artificial intelligence solution is provided to predict the non-deterministic characteristics of RCS using the supervised machine learning algorithm that involves Gaussian process (GP) regression. A parametrised aircraft model is used to generate training data where five variables are selected as predictors while the response is chosen to be monostatic RCS in the azimuth plane. To provide a comparison of GP modelling-based predictions, shooting and bouncing rays-based multi-frequency RCS simulations are used and the results show good agreement. To further validate the GP-based modelling approach, the data of a design point is compared with the measured RCS of 1:8 scaled-down aircraft model, which confirms the accuracy of the proposed methodology. Good prediction capabilities of GP regression for RCS evaluation of complex geometries and requirement of small data set make it an excellent tool for exploring the large design space as well as integration into multi-disciplinary design optimisation environments.

1 Introduction

Radar cross-section (RCS) has found numerous applications in modern technologies such as active missile systems, lidars, target detection and monitoring in the Internet of Things (IoT), human breath rate detection, stealth aircraft and satellite design etc. [1–6]. In addition to achieving low observability, it plays a critical role in designing a number of electronic warfare systems, for instance radars, jammers and radar warning receivers [7–11]. Computing the RCS of electrically large structures is a complex process that requires large amounts of memory and computation time [7, 12]. These requirements are even greater when simulations are carried out for design space exploration in multi-disciplinary design optimisation. RCS variables can be broadly classified into two categories: simulation parameters (frequency, polarisation etc.) and geometric parameters (wing sweep angle, dihedral angle etc.). Variation in most of these parameters affects RCS in a complex manner, for example when the angle of incidence is changed, the generated RCS plot is quite complex and can be regarded as random [13].

To compute RCS of complex geometries across a large design space, artificial intelligence has the potential of providing a viable solution. It has previously been used to predict RCS as a function of frequency by Jacobs and du Plessis. [14], who have carried out a multi-frequency analysis to predict the RCS of a missile at one incident angle. Owing to the quasi-periodic nature of the response, Jacobs and du Plessis [14] have used a composite kernel covariance function for Gaussian process (GP) modelling of RCS. As there was only one predictor (frequency), the training time for the model was considerably less. In related work, Jacobs and du Plessis [15] have used the same composite kernel function for modelling the aperture efficiency and squared-exponential covariance function for predicting antenna scattering parameters (S_{11}) [16]. In all of these references [14–16], only one predictor (i.e. frequency) was used. However, in reality, the number of geometric and simulation parameters affect RCS in a random manner and therefore, it becomes essential to use a kernel function which is applicable for aperiodic responses and requires a separate kernel length scale for each variable.

Simulation parameters (e.g. frequency, angle of incidence etc.) and geometric parameters (e.g. wing sweep angle, dihedral angle etc.) form a very complex mesh in three-dimensional space as depicted in Fig. 1.

In this work, a design space defined by the upper and lower bounds of four key geometric variables is explored at multiple frequencies by computing RCS in azimuth plane using shooting and bouncing rays (SBR) [17] simulations. Subsequently, the results are used as training data for GP modelling to predict RCS at intermediate design points. All of the geometric parameters in this study are seen to produce an aperiodic RCS response. Therefore, instead of composite kernel covariance function, Matern 5/2 covariance function was used with four separate kernel length scales.

Section 2 outlines a brief mathematical background of used kernel covariance function and kernel scales. SBR simulations as a function of geometric variables and angles of incidence show the aperiodic nature of monostatic RCS. Section 3 presents the comparison of GP modelling and SBR simulations at one design point and multiple frequencies. Comparison of root mean square error (RMSE) of the GP model for 16 randomly selected design points is also shown. Data of one design point was used to fabricate a 1:8 scaled-down aircraft model and its RCS was measured in an anechoic chamber and compared with the predicted RCS. Section 4 provides a conclusion to this research work.

2 Background

2.1 GP regression overview

In regression modelling, a kernel function is a key element that describes the covariance of a random variable. Changing the kernel function changes the prior, and hence, changing the model response. Based on the underlying physics, the responses vary with respect to the predictors and various kernel functions have been proposed for modelling of different response types [18, 19]. For modelling of quasi-periodic responses, Jacobsand du Plessis [14] have proposed a composite covariance function (1) which is a product of two covariance functions that are in the same space:

$$k(x, x') = \left(\sigma_f^2\right)^2 \mathrm{e}^{\frac{(\sin[\pi|x-x'|/\lambda])^2}{\theta^2} + \sum_{k=1}^{D} \frac{(x_k - x_k')^2}{\tau_k^2}} \quad (1)$$

where σ_f^2 is the maximum allowable covariance, λ the period of the quasi-periodic response, θ the length scale for periodic component and τ_k the length scale for aperiodic component.

These length scales change the effectiveness of the distance between the training and testing data. This approach takes into account the periodicity of RCS responses through the hyperparameter λ.

Fig. 2 shows the quasi-periodic RCS response when the frequency is taken as the predictor. On the other hand, once RCS response is evaluated for varying geometric parameters, it becomes completely aperiodic as shown in Fig. 3. In addition, since we are dealing with multiple parameters, a multivariate statistical analysis is required that encompasses this variation. We disregard any trends or periodicity in the data and use the Matérn covariance function, which is positive semi-definite, to model RCS as a function of geometric variables. The choice was made on the basis of the differentiability and stationary property of the function and a special case of Matérn 5/2 was employed which is as follows:

$$k(x, x') = \sigma_f^2 \, \mathrm{e}^{-\sqrt{5}r}\left(1 + \sqrt{5}r + \frac{5}{3}r^2\right) \tag{2}$$

Length scales for each predictor are embedded in the variable ' r ' (3) and are used to scale the distance between the training and testing data:

$$r = \sqrt{\sum_{k=1}^{D} \frac{(x_k - x_k')^2}{\tau_k^2}} \tag{3}$$

The kernel length scale τ_k takes on a new value for each predictor. Hence, the use of multiple predictors increases the number of computations required to calculate each element of the kernel matrix given in (4):

$$\boldsymbol{K} = \begin{bmatrix} k(x_1, x_1) & \cdots & k(x_1, x_n) \\ \vdots & \ddots & \vdots \\ k(x_n, x_1) & \cdots & k(x_n, x_n) \end{bmatrix} \tag{4}$$

$$\boldsymbol{K}' = \begin{bmatrix} k(x', x_1) & k(x', x_2) & \ldots & k(x', x_n) \end{bmatrix} \tag{5}$$

$$\boldsymbol{K}'' = k(x', x') \tag{6}$$

The matrices in (4)–(6) are used to compute the mean and variance of the established Gaussian distribution given by

$$x' \big| \boldsymbol{x} \sim \mathcal{N}\left(\boldsymbol{K}'\boldsymbol{K}^{-1}\boldsymbol{x}, \; \boldsymbol{K}'' - \boldsymbol{K}'\boldsymbol{K}^{-1}\boldsymbol{K}'^{\mathrm{T}}\right) \tag{7}$$

This approach works because the training data is assumed to be a subset of a multi-variate Gaussian distribution and the hyperparameters σ_f^2 and τ_k are optimised as shown by Williams and Rasmussen [18]. It drastically increases the computation time as seen from the elements of the kernel matrix and from the mean and variance of the modelled distribution but once the response surface is constructed, RCS can be accurately predicted, hence making this approach suitable for integration in multi-disciplinary modelling and simulation environments. Several machine learning approaches have previously been applied to address various problems such as target classification [20], image de-noising [21], detection of unmanned aerial vehicles [22], ship size extraction [23] and significant wave height estimation [24]. However, this method in particular, can be utilised in the applications where RCS optimisation with respect to geometric parameters is required such as stealth aircrafts, ships and satellite design. In IoT, this approach can be used to model human targets as a function of the movement of their body parts while as part of biomedical applications, it can be used to estimate the breathing rate by quantifying the variation in RCS as a function of chest movement [5]. In addition, a similar approach can be devised to predict RCS and use it for synthetic aperture radar imaging or to predict antenna scattering field distributions.

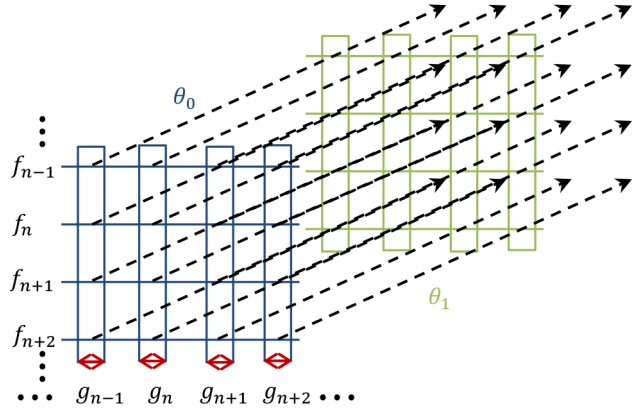

Fig. 1 *Depiction of RCS as a function of frequency f_n, angle of incidence θ_n and geometric parameters g_n, where each g_n spans a space while f_n and θ_n take a pre-defined value*

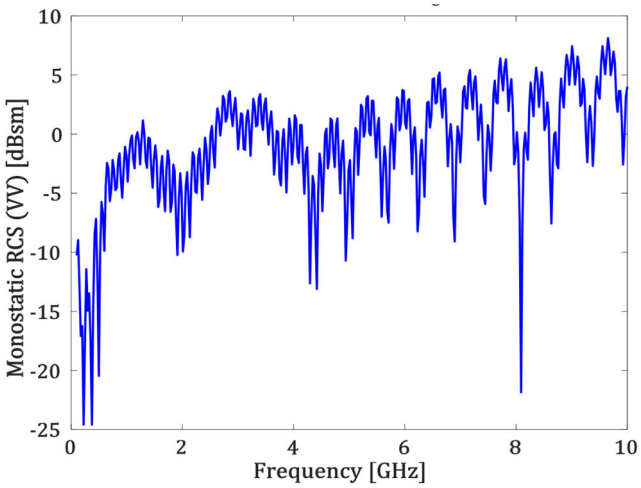

Fig. 2 *Quasi-periodic RCS responses as a function of frequency at one incident angle*

2.2 k-fold cross-validation

To validate the accuracy, modelled responses are cross-validated using various methods depending on the size and type of the data set. We have employed a *k*-fold cross-validation method because, in our case, generating training data is computationally expensive and this method leaves enough data for validation. Specifically, for each frequency and angle of incidence, we have divided our design points into five folds where four of them are used for modelling while the fifth one is used for validation and regression loss computation. Fig. 4 shows one such validation whose mean regression loss is 1.59 at 0° angle of incidence.

3 Results and discussion

3.1 Simulation versus prediction

The geometric parameters that are used for the comparison of simulated and predicted RCS responses are shown in Fig. 5. These variables are an integral part of the aircraft design process because they play a key role in determining stealth as well as manoeuvrability. The design space around this variable is defined by specifying the upper and lower bounds of these variables. These bounds are limited by aircraft performance requirements and constraints.

Besides the geometric parameters, the frequency and angle of the incident wavefront are also varied to obtain a complete azimuth plane RCS response. Simulations are done using the SBR technique in VV polarisation at 0.5, 1, 1.5 and 2 GHz. To include diffraction effects, the physical theory of diffraction was incorporated with a ray density of ten edge segments per wavelength.

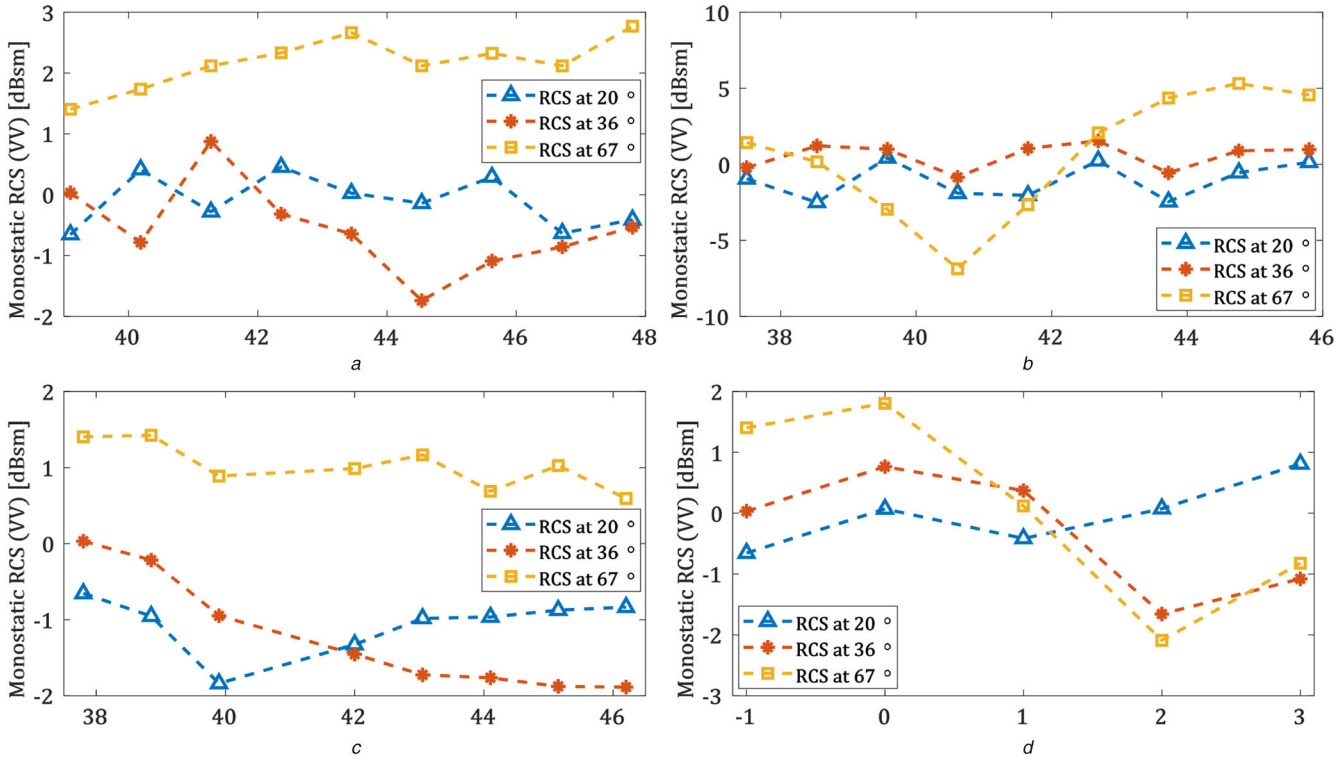

Fig. 3 *Variations in monostatic RCS at 1 GHz VV polarisation when all the geometric variables are fixed except* ***(a)*** Wing sweep angle, ***(b)*** Tail sweep angle, ***(c)*** Horizontal tail sweep angle, ***(d)*** Dihedral angle

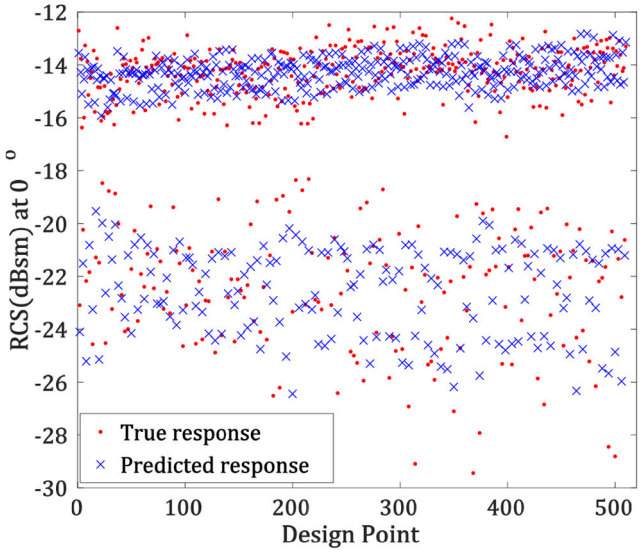

Fig. 4 *Five-fold cross-validation at 0.5 GHz*

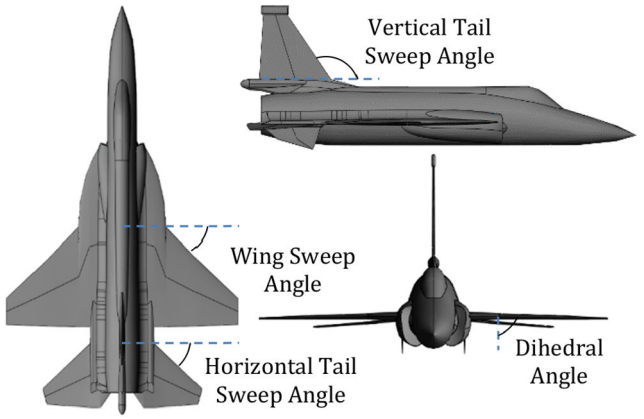

Fig. 5 *Geometric parameters of an aircraft model taken as predictors*

A total of 510 combinations of geometric parameters, 181 incident angles and 4 frequencies defined the entire design space on which the training data was generated. All the simulations and training were done on Intel E5-2620 workstation with 16 Xeon processors of 2.1 GHz clock frequency. Using all processors in parallel, the training time for the GP model was 29 min.

After the development of the trained model, RCS was predicted at a new design point (dihedral angle 0°, wing sweep angle 44°, horizontal tail sweep angle 47° and vertical tail sweep angle 43°) and compared with the simulated RCS, as shown in Fig. 6. In these polar charts, 0° and 180° correspond to the front (radome) and rear (tail) sections of the aircraft model, respectively. Owing to the symmetry in the aircraft structure, only half of the pattern is shown here.

It is evident from the comparison that the RCS pattern predicted using the trained model highly correlates with that of the actual SBR simulations. Despite the sudden fluctuations in RCS as a function of angle of incidence, the GP model accurately predicts the RCS responses. For example, in the range of 30–60°, RCS variation is very high but the output of the trained model closely predicts the RCS response for all four frequencies (see the inset in Figs. 6*a–d*).

A new set of 16 design points (random combinations of geometric variables) was used for SBR simulations and GP model predictions. The RMSE of simulated and predicted responses for these design points was computed using (8) and is shown in Fig. 7:

$$\text{RMSE} = \sqrt{\frac{1}{N_{\text{inc}}}\sum_{N_{\text{inc}}}(\sigma_{\text{s}} - \sigma_{\text{p}})^2} \tag{8}$$

where σ_{s} is the simulated RCS using SBR, the predicted RCS using GP modelling and N_{inc} the number of incident directions.

Values of mean error are listed in Table 1. Out of the four frequencies of interest, RMSE has a maximum mean value at 1.5 GHz, which is 3.8 dBsm. Across all design points and frequencies, the maximum RMSE is only 5 dBsm which is at 1.5 GHz. Since RCS magnitude has a higher dynamic range and fluctuates more at higher frequencies, the prediction model is likely to be more error prone. In simple words, the RMSE should be greater at higher frequencies but Fig. 7 shows that RMSE shows no such behaviour.

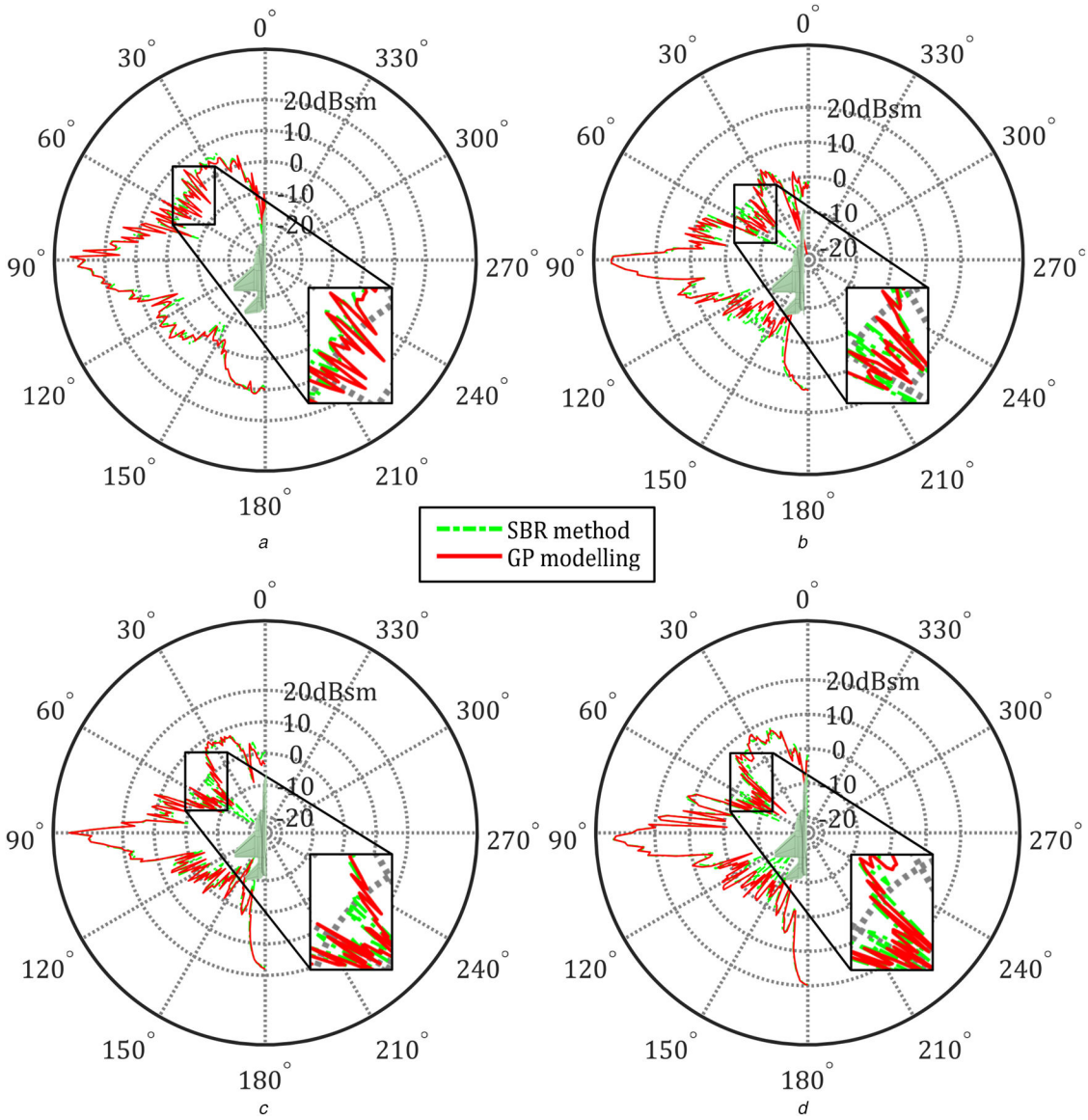

Fig. 6 *Comparison of simulated (SBR) and predicted (GP) RCS (dBsm) at one design point in VV polarisation at* ***(a)*** 0.5 GHz, ***(b)*** 1 GHz, ***(c)*** 1.5 GHz, ***(d)*** 2 GHz

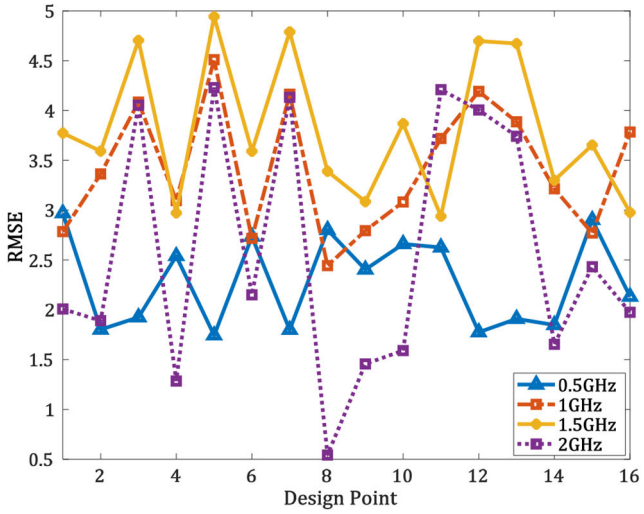

Fig. 7 *Comparison of RMSE of GP model for 16 randomly selected design points*

This may be owing to the fact that the regression model for each frequency has been trained independently. Therefore, the model encompasses the fluctuations that arise at that particular frequency. This also implies that the trained model becomes more and more complex with an increase in frequency.

3.2 Comparison of predicted and measured RCS

To experimentally validate the RCS response predicted by the GP model, the data of one design point was used to fabricate 1:8 scaled-down aircraft model. The model was manufactured on a five-axis computer numerical control (CNC) machine using Edaboard 60-1 (chemical wood) and coated with CHO-SHIELD® 4900 electrically conductive paint.

Fig. 8 shows the fabricated model mounted on a pylon inside the test chamber whose walls are mounted with broadband absorbers. Styrofoam is used to cover the pylon so that it does not affect the RCS measurement. The test chamber has a dual reflector where the dimensions of the reflector antenna are 15 × 8 × 6 ft and supports a frequency range of up to 20 GHz.

Fig. 9 shows the mean RCS values of SBR simulations, GP model predictions and anechoic chamber measurements. It may be noted that all three values (for each frequency) agree with each other within the uncertainty bounds. However, the GP model prediction matches more closely with experimental measurements.

Fig. 10 shows the detailed comparison of measured and simulated RCS to the predicted RCS at this design point (dihedral angle 0°, wing sweep angle 43.44°, horizontal tail sweep angle 42° and vertical tail sweep angle 41.68°). It is to be noted that antenna

Table 1 Mean error of 16 randomly selected design points

frequency, GHz	0.5	1.0	1.5	2.0
mean error, dBsm	2.28	3.4	3.8	2.58

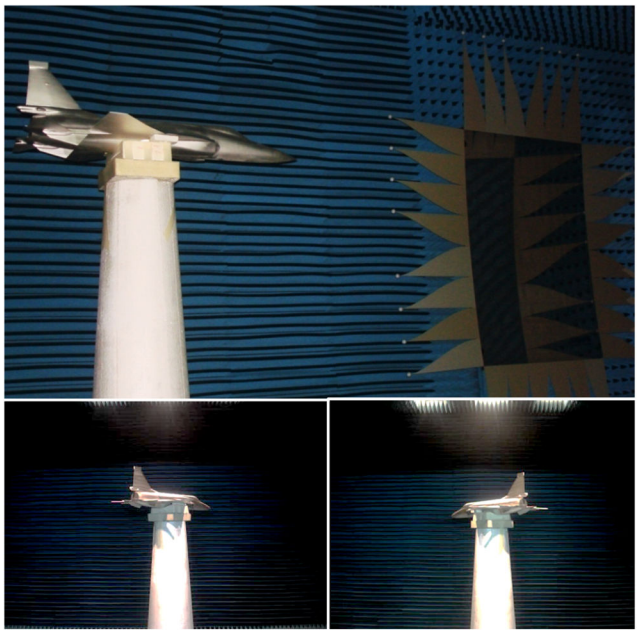

Fig. 8 *Experimental setup for RCS measurement*

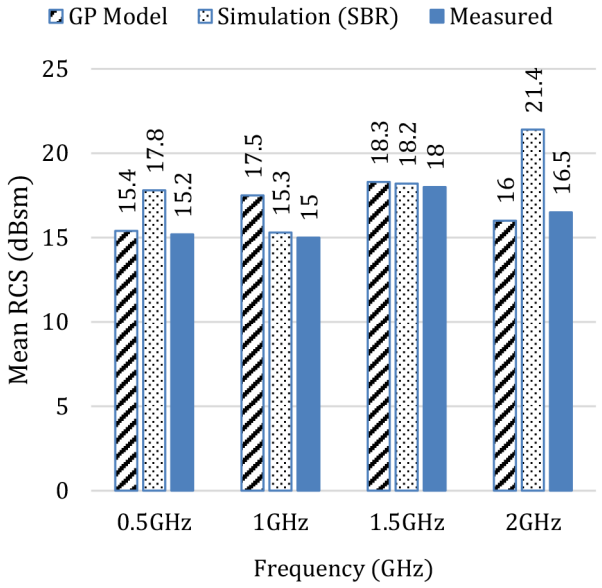

Fig. 9 *Mean RCS (dBsm) comparison between GP modelling, simulation and experimental results*

mode scattering is not taken into account because the fighter aircraft model does not have a nose radar. The peak value of RCS amplitude is at 90° azimuth because of the maximum projected area. It is evident from Fig. 10 that RCS predictions of the GP model are in good agreement with the measured RCS. Hence, it can be inferred that this prediction approach of multi-variate Gaussian distribution can be used to model RCS magnitude at multiple frequencies.

4 Conclusion

RCS signature is an important parameter in the design of stealth aircrafts, ships and satellites. There are several geometric parameters that affect the RCS in a random manner, which complicates the modelling and simulation environment and results in the high computational cost. To efficiently overcome these constraints, a supervised learning-based approach involving GP is proposed to accurately predict the RCS in the given design space. At first, RCS magnitude as a function of geometric variable was computed and used to train a regression model. After *k*-fold cross-validation, this trained model was used to make predictions within the design space and the predicted responses were compared with the computed RCS obtained from the SBR method. To quantify the performance of the proposed modelling approach, RMSE was evaluated and a mean error of 3.8 dBsm was observed which shows a close match between the predicted and computed RCS. For experimental validation, a 1:8 scaled-down aircraft model was manufactured and its RCS was measured in an anechoic chamber which was compared with the predicted RCS and the two results showed good agreement across all frequencies. It is, therefore, concluded that a GP regression-based prediction model can reliably be used for RCS estimation of complex geometries. This approach can be expanded to include more simulation and geometric parameters for RCS optimisation in multi-disciplinary design

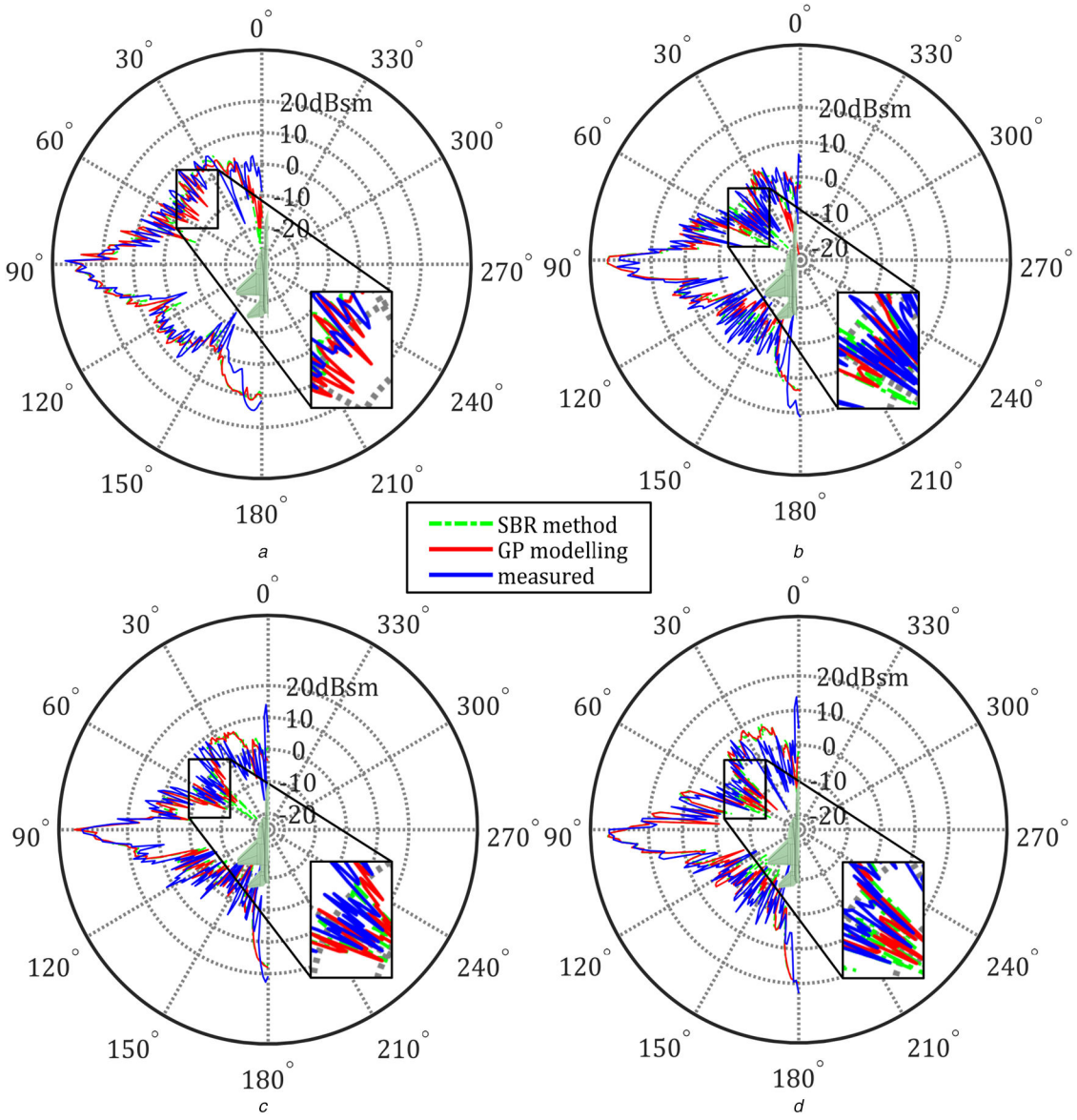

Fig. 10 *Comparison of measured and simulated versus predicted RCS (dBsm) in azimuth plane at one design point in VV polarisation at* ***(a)*** 0.5 GHz, ***(b)*** 1 GHz, ***(c)*** 1.5 GHz, ***(d)*** 2 GHz

exploration. A similar methodology may also be used for the generation of scattering field for antenna applications.

5 References

[1] Greving, G., Biermann, W.D.: 'Application of the radar cross section RCS for objects on the ground − example of wind turbines'. IEEE Int. Radar Symp., Wroclaw, Poland, May 2008, pp. 1–4

[2] Belgiovane, D., Chen, C.C., Chen, M., *et al.*: '77 GHz radar scattering properties of pedestrians'. IEEE Radar Conf., Cincinnati, OH, USA., May 2014, pp. 0735–0738

[3] Wen, C., Zhu, J., Zhou, Y., *et al.*: 'Study on ISAR imaging for forward-looking missile-borne millimetre wave radar', *J. Eng.*, 2019, **2019**, (20), pp. 6718–6722

[4] Jenn, D.C.: '*Radar and laser cross section engineering*' (American Institute of Aeronautics and Astronautics, Inc., Reston, VA, USA., 2019)

[5] Piuzzi, E., D'Atanasio, P., Pisa, S., *et al.*: 'Complex radar cross section measurements of the human body for breath-activity monitoring applications', *IEEE Trans. Instrum. Meas.*, 2015, **64**, (8), pp. 2247–2258

[6] Yang, F., He, Z., Fu, Y., *et al.*: 'Noncontact detection of respiration rate based on forward scatter radar', *Sensors*, 2019, **19**, (21), p. 4778

[7] Knott, E.F.: '*Radar cross section measurements*' (Springer Science & Business Media, Berlin, Germany, 2012)

[8] Martorella, M.: '*Multidimensional radar imaging*' (SciTech Publishing, an imprint of The Institution of Engineering and Technology, Stevenage, 2019)

[9] Peterson, J.: 'Overview of low observable technology and its effects on combat aircraft survivability', *J. Aircr.*, 1999, **36**, (2), pp. 380–388

[10] Whitford, R.: 'Designing for stealth in fighter aircraft (stealth from the aircraft designer's viewpoint)'. SAE Technical Paper, No. 965540, October 1996

[11] Narayanan, R.M., Allebach, J.M., Himed, B.: 'Comparison of noise and chirp waveforms for radar target detection in clutter', *IET Radar Sonar Navig.*, 2019, **13**, (8), pp. 1333–1343

[12] Smit, J.C., Cilliers, J.E., Burger, E.H.: 'Comparison of MLFMM, PO and SBR for RCS investigations in radar applications'. IET Int. Conf. on Radar Systems, Glasgow, UK., 2012

[13] Budge, M.C., German, S.R.: '*Basic RADAR analysis*' (Artech House, Massachusetts, MA, USA., 2015)

[14] Jacobs, J.P., du Plessis, W.P.: 'High-accuracy Gaussian process modelling of missile RCS with cost-based preferential training data selection'. 12th European Conf. on Antennas and Propagation, London, UK., 2018

[15] Jacobs, J.P., de Villiers, D.I.: 'Gaussian process modeling of aperture efficiency ripple in reflector antennas'. Loughborough Antennas and Propagation Conf., Loughborough, UK., November 2015, pp. 1–4

[16] Jacobs, J.P., Koziel, S.: 'Two-stage framework for efficient Gaussian process modeling of antenna input characteristics', *IEEE Trans. Antennas Propag.*, 2013, **62**, (2), pp. 706–713

[17] Bilal, A., Hamza, S.M., Taj, Z., *et al.*: 'Comparison of SBR and MLFMM techniques for the computation of RCS of a fighter aircraft', *IET Radar Sonar Navig.*, 2019, **13**, (10), pp. 1805–1810

[18] Williams, C.K., Rasmussen, C.E.: '*Gaussian processes for machine learning*' (MIT Press, Cambridge, MA, 2006)

[19] Minasny, B., McBratney, A.B.: 'The mateatrn function as a general model for soil variograms', *Geoderma*, 2005, **128**, (3–4), pp. 192–207

[20] Lee, K.-C.: 'Radar target recognition by machine learning of K-nearest neighbors regression on angular diversity RCS', *Appl. Comput. Electromagn. Soc. J.*, 2019, **34**, (1), pp. 75–81

[21] Bai, X., Peng, X.: 'Radar image series denoising of space targets based on Gaussian process regression', *IEEE Trans. Geosci. Remote Sens.*, 2019, **57**, (7), pp. 4659–4669

[22] Farlik, J., *et al.*: 'Radar cross section and detection of small unmanned aerial vehicles'. 17th IEEE Int. Conf. on Mechatronics-Mechatronika (ME), Prague, Czech Republic, December 2016, pp. 1–7

[23] Li, B., Liu, B., Guo, W., *et al.*: 'Ship size extraction for Sentinel-1 images based on dual-polarization fusion and nonlinear regression: push error under one pixel', *IEEE Trans. Geosci. Remote Sens.*, 2018, **56**, (8), pp. 4887–4905

[24] Cornejo-Bueno, L., Nieto Borge, J.C., Alexandre, E., *et al.*: 'Accurate estimation of significant wave height with support vector regression algorithms and marine radar images', *Coastal Eng.*, 2016, **114**, pp. 233–243